JPn Neuroscience

The Journal of Physiology

J Physiol 591.13 (2013) pp 3433–3449

Enhanced inhibitory neurotransmission in the cerebellar cortex of *Atp1a3*-deficient heterozygous mice

Keiko Ikeda[1,2,5], Shin'Ichiro Satake[2], Tatsushi Onaka[3], Hiroki Sugimoto[1], Naoki Takeda[4], Keiji Imoto[2] and Kiyoshi Kawakami[1]

[1]*Division of Biology, Center for Molecular Medicine, Jichi Medical University, Yakushiji 3311-1, Shimotsuke, Tochigi 329-0498, Japan*
[2]*Department of Information Physiology, National Institute for Physiological Sciences (NIPS), and School of Life Science, The Graduate University for Advanced Studies (SOKENDAI), Higashiyama 5-1, Myodaiji, Okazaki, Aichi 444-8787, Japan*
[3]*Department of Physiology, School of Medicine, Jichi Medical University, Japan*
[4]*Center for Animal Resources and Development (CARD), Kumamoto University, Honjo 2-2-1, Kumamoto 860-0811, Japan*
[5]*Biology, Hyogo College of Medicine, Mukogawa 1-1, Nishinomiya, Hyogo 663-8501, Japan*

Key points

- Mutations of *ATP1A3* cause rapid-onset dystonia with parkinsonism (RDP) and alternating hemiplegia of childhood (AHC).
- The mRNA of *Atp1a3* was highly expressed in molecular-layer interneurons and Purkinje cells in the developing mouse cerebellar cortex, and the gene product was observed as dots in the molecular layer, on the surface of Purkinje cell soma and the pinceaux.
- Here we report that *Atp1a3*$^{+/-}$ mice showed increased symptoms of dystonia when being administrated kainate into cerebellum. We also found enhanced inhibitory neurotransmission between molecular-layer interneurons and Purkinje cells in the developing cerebellum of *Atp1a3*$^{+/-}$ mice.
- These findings suggest that *ATP1A3* haploinsufficiency in the cerebellum has some effect on the inhibitory, but not the excitatory, circuitry and the interaction among different cell types during development. Disturbances of the cerebellar inhibitory network seem to be the underlying pathophysiological mechanism of dystonia among the increasing spectrum of complex neurological symptoms in RDP and AHC.

Abstract Dystonia is characterized by excessive involuntary and prolonged simultaneous contractions of both agonist and antagonist muscles. Although the basal ganglia have long been proposed as the primary region, recent studies indicated that the cerebellum also plays a key role in the expression of dystonia. One hereditary form of dystonia, rapid-onset dystonia with parkinsonism (RDP), is caused by loss of function mutations of the gene for the Na pump α3 subunit (*ATP1A3*). Little information is available on the affected brain regions and mechanism for dystonia by the mutations in RDP. The Na pump is composed of α and β subunits and maintains ionic gradients of Na^+ and K^+ across the cell membrane. The gradients are utilized for neurotransmitter reuptake and their alteration modulates neural excitability. To provide insight into the molecular aetiology of RDP, we generated and analysed knockout heterozygous mice (*Atp1a3*$^{+/-}$). *Atp1a3*$^{+/-}$ showed increased symptoms of dystonia that is induced by kainate injection into the cerebellar vermis. *Atp1a3* mRNA was highly expressed in Purkinje cells and molecular-layer interneurons, and its product was concentrated at Purkinje cell soma, the site of abundant vesicular γ-aminobutyric acid transporter (VGAT) signal, suggesting the presynaptic localization of the α3 subunit in the inhibitory synapse. Electrophysiological studies showed that the inhibitory neurotransmission

DOI: 10.1113/jphysiol.2012.247817

at molecular-layer interneuron–Purkinje cell synapses was enhanced in *Atp1a3*$^{+/-}$ cerebellar cortex, and that the enhancement originated via a presynaptic mechanism. Our results shed light on the role of *Atp1a3* in the inhibitory synapse, and potential involvement of inhibitory synaptic dysfunction for the pathophysiology of dystonia.

(Received 12 November 2012; accepted after revision 1 May 2013; first published online 7 May 2013)

Corresponding authors K. Kawakami or K. Ikeda: Division of Biology, Center for Molecular Medicine, Jichi Medical University, Yakushiji 3311-1, Shimotsuke, Tochigi 329-0498, Japan. Email: kkawakam@jichi.ac.jp or kiikeda@hyo-med.ac.jp

Abbreviations ACSF, artificial cerebrospinal fluid; AHC, alternating hemiplegia of childhood; AIDA, (*RS*)-1-aminoindan-1,5-dicarboxylic acid; *ATP1A3* or *Atp1a3*, the gene for Na pump α3 subunit; *Atp1a3*$^{+/-}$, heterozygous gene-knockout mice of *Atp1a3*; CF, climbing fibre; CN, cerebellar nuclei; CNQX, 6-cyano-7-nitroquinoxaline-2,3-dione; DAPI, 4,6-diamidino-2-phenylindole; E, embryonic day; EGFP, enhanced green fluorescent protein; E_m, membrane potential; EPSC, excitatory postsynaptic current; ES, embryonic stem; G, gauge; GAD, glutamate decarboxylase; γ-DGG, γ-D-glutamylglycine; GL, granular layer; mIPSC, miniature inhibitory post-synaptic current; ML, molecular layer; PC, Purkinje cell; PCL, Purkinje cell layer; P, postnatal day; PF, parallel fibre; PGK, phosphoglycerate kinase; PPR, paired-pulse ratio; RDP, rapid-onset dystonia with parkinsonism; *tg*, tottering; TTX, tetrodotoxin; VGAT, vesicular γ-aminobutyric acid transporter; VGLUT 1/2, vesicular glutamate transporter 1/2; WM, white matter; WT, wild-type littermate.

Introduction

Na,K-ATPase (Na pump) is the enzyme responsible for the maintenance of electrochemical gradients of Na^+ and K^+ across the animal cell membrane. The pump is composed of α and β subunits. The catalytic α subunit contains the binding sites for the cations, ATP and specific inhibitor of ouabain (Lingrel & Kuntzweiler, 1994). Four α subunit isoforms (α1, α2, α3 and α4) are encoded by different genes in mammals. Each α isoform is expressed in a tissue-specific manner and shows differences in kinetic properties and substrate affinities (Jewell & Lingrel, 1991; Segall *et al.* 2001; Blanco, 2005).

The gene for the human Na pump α3 subunit, *ATP1A3*, has been identified as the causative gene for *DYT12*, rapid-onset dystonia with parkinsonism (RDP) (de Carvalho Aguiar *et al.* 2004; Brashear *et al.* 2007). The mutations identified in patients cause dysfunction of the transport activity of the Na pump (Rodacker *et al.* 2006; Blanco-Arias *et al.* 2009). Therefore, haploinsufficiency of the gene dosage is thought to contribute to RDP. Recently, heterozygous mutations in *ATP1A3* were found in alternating hemiplegia of childhood (AHC) (Heinzen *et al.* 2012; Rosewich *et al.* 2012). The clinical characteristics of *DYT12* and AHC overlap considerably, indicating different manifestations along a clinical spectrum (Ozelius, 2012).

Dystonia is a central symptom of RDP and is manifested in some AHC patients, and dystonia itself is a relatively common neurological disorder characterized by excessive involuntary muscle contractions and prolonged simultaneous contraction of both agonist and antagonist muscles, often leading to twisting movements or abnormal posture (Phukan *et al.* 2011). Although the basal ganglia have been proposed as the primary regions responsible for the expression of dystonia, recent studies have reported that the cerebellum also plays a critical role (Campbell & Hess, 1998; Pizoli *et al.* 2002; Neychev *et al.* 2008, 2011; Niethammer *et al.* 2011). For example, tottering (*tg*) mice harbouring a mutation in the α_{1A} subunit of the voltage-sensitive P/Q-type calcium channel gene showed spontaneous dystonia (Campbell & Hess, 1998, 1999) and abnormal cerebellar synaptic transmission (Matsushita *et al.* 2002). Dystonia is eliminated by surgical removal of the cerebellum in *tg* mice (Neychev *et al.* 2008). In addition, another recent study, in which dystonia was induced in mice by injecting ouabain into both the cerebellum and/or the basal ganglia, showed that the primary site for initiation of dystonia is the cerebellum, aberrant activity of which altered the function of basal ganglia and resulted in the manifestation of dystonia symptoms (Calderon *et al.* 2011). Thus, the pathogenesis of dystonia of RDP can be considered to involve abnormal neural circuitry in the cerebellum. In this regard, it is important to identify defects in the cerebellum at neuronal cell level and at neuronal network level that contribute to the development of RDP as a primary site.

In this study, we generated a new mouse line harbouring a deletion mutation of the *Atp1a3* gene. We thoroughly examined properties of the synaptic transmission onto Purkinje cells (PCs) and distribution of the Na pump α subunits in the cerebellum. The results showed a significant enhancement of the inhibitory synaptic transmission in heterozygous mice, and high expression of *Atp1a3* in inhibitory neurons, with accumulation of its product at the presynaptic structure. This is the first comprehensive report of synaptic transmission in the cerebellum of *Atp1a3* mutant mice, and the present findings emphasize the significant function of *Atp1a3* in inhibitory synapses in the cerebellar cortex, and shed light

on possible involvement of inhibitory synapses on dystonia symptoms.

Methods

Animal experiment ethics

All experimental protocols described in the present study were carried out in accordance with the institutional guidelines for animal experiments and approved by the Ethics Review Committee for Animal Experimentation of Jichi Medical University and National Institute for Physiological Science (NIPS).

Construction of *Atp1a3* targeting vector and generation of *Atp1a3* mutant mice

Mouse genomic DNA containing exons 1–8 of *Atp1a3* was isolated by screening the C57BL/6 mouse genomic λDASHII library (Stratagene, La Jolla, CA, USA) using a mouse *Atp1a3* cDNA probe [nucleotide positions 1–976 (position 1 as initiating methionine codon)]. Several genomic DNA fragments covering a region of approximately 10,000 bp upstream and downstream of exon 1 were isolated and subcloned into pBlueScript KS (Stratagene). For construction of a plasmid coding for the Na pump α3 subunit–enhanced green fluorescent protein (EGFP) fusion protein, the whole coding sequence of *Atp1a3* was subcloned into *Hin*dIII–*Not*I site of the pCMV26 vector (Sigma-Aldrich, St Louis, MO, USA) followed by insertion of the *EGFP* coding sequence into the *Eco*RV site. EGFP was fused to the carboxy terminal of the Na pump α3 subunit, because we primarily intended to monitor the intracellular localization of the subunit by fluorescence. The loxP sequence was inserted at the *Bst*EII site of the long arm (8609 *Eco*RI to 13,574 *Not*I site). The bacterial diphtheria toxin α subunit gene (DTA in Fig. 1) driven by the phosphoglycerate kinase (PGK) I gene promoter was inserted downstream of the short arm (17,288 *Pvu*II site to 19,931 *Afl*II site). The STOP-polyA sequence was inserted downstream of the short arm. The PGKneobpA cassette (Fig. 1) flanked by FRT sequence

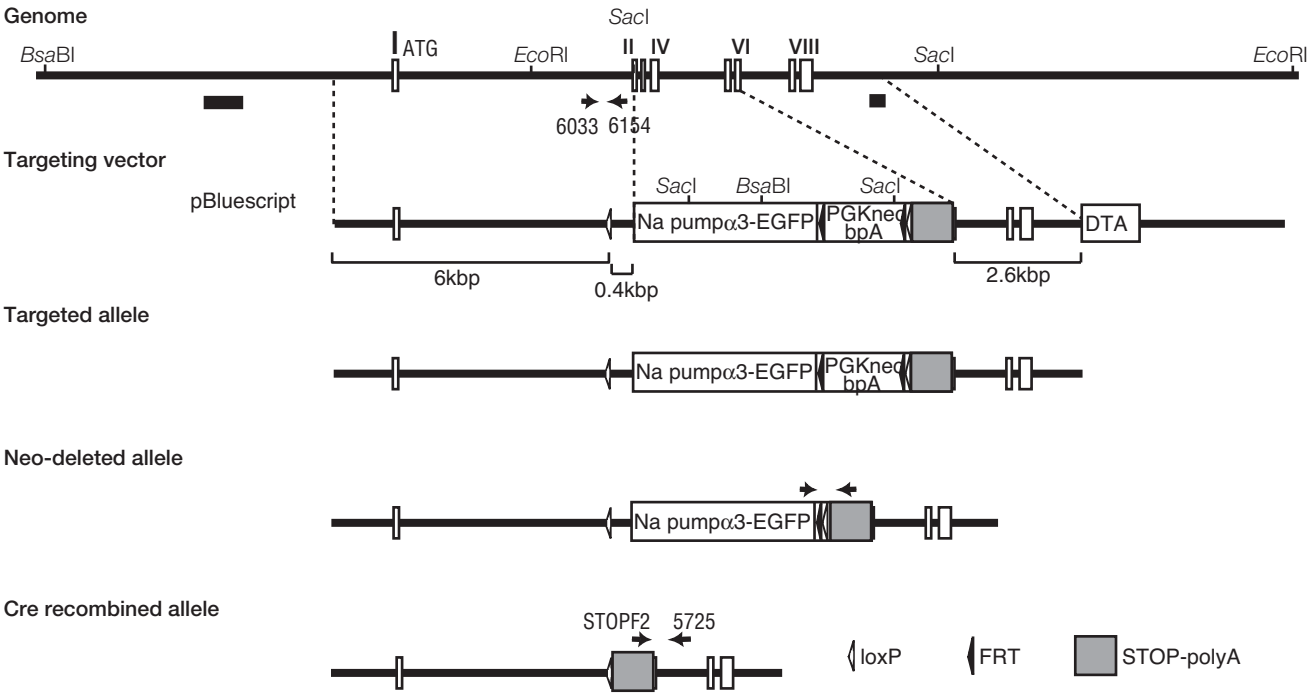

Figure 1. Targeting strategy for mutating the Na pump α3 subunit gene (*Atp1a3*)
Genome scheme with restriction enzyme sites in the uppermost part of the figure. The N-terminal exons of *Atp1a3* (exons I–VIII) appear in white boxes. The coding sequence of *Atp1a3* plus enhanced green fluorescent protein (EGFP) gene, followed by a neomycin-resistant gene cassette (PGKneobpA, depicted as a white box), flanked by FRT sequences, loxP site and STOP-polyA cassette were replaced to the covering region between exon 2 (II) and exon 6 (VI). A bacterial diphtheria toxin subunit gene (DTA, depicted as a white box) was inserted for negative selection. Southern probes used for Southern blot analyses of genomic DNA appear in the black thick bars in the uppermost part of the figure. The process used to obtain the mutant allele is described in the Methods. Neo-deleted alleles were verified by PCR using the set of primers described by the arrows on the fourth line from the top. The targeted mutant allele, i.e. cre recombined allele, was verified by PCR using primers STOPF2 and 5725 (arrows on the fifth line from the top). The inserted loxP sites and FRT sites are shown as open and filled triangles, respectively.

with downstream loxP site was inserted downstream of the Na pump α3 subunit–EGFP fusion protein coding sequence. Embryonic stem (ES) cells (TT2 ES cell line) were electroporated with the linearized targeting vector as described previously (Yagi *et al.* 1993). G418-resistant ES clones were screened by PCR using primers 6033 (5′-GGGTTTTCCTCTTAGCCTGGTGAC-3′) and 6154 (5′-TGTTTGTGTGGAGGTCAGAGGATAG-3′). Homologous recombinant candidates were verified by Southern hybridization using the probes (5828 *Pvu*II to 6634 *Bgl*II fragment for the 5′ terminal external probe and 19931 *Afl*II to 20,200 *Bsa*I for the 3′ terminal external probe) shown in Fig. 1. Chimeras were generated by injecting the recombinant ES cells into ICR 8 cell embryos and transferred to ICR (CD-1, Charles River Japan, Inc., Tokyo, Japan) foster mothers. Unfortunately, the resulting heterozygous mice ($Atp1a3^{+/EGFP}$) did not show any expression of the α3 subunit–EGFP fusion protein in the brain, probably because of degradation of the fusion protein. We could not detect the expression of the fusion protein by fluorescence and therefore did not use the mice for further analyses. The *Atp1a3-EGFP* gene knock-in allele was excised by crossing ubiquitously expressing Cre mice, and the germ line deletion of the *Atp1a3* locus was selected and backcrossed to C57BL/6J (CLEA Japan, Inc., Tokyo, Japan) for 7–20 generations. Heterozygous gene-knockout mice of *Atp1a3* ($Atp1a3^{+/-}$) were identified using primers (6033 and 6154) for the wild-type allele described above and primers (STOPF2, 5′-CATACTGTTTTTTCTTACTCCACACAGGCA-3′; 5725, 5′-CACACACACACACAAAAGCTGGACATGG-3′) for the mutant-type allele. In every experiment, mice from each genotype were littermates of the isogenic genetic background. The low expression level of *Atp1a3* mRNA in the cerebellum of $Atp1a3^{+/-}$ mice was confirmed by *in situ* hybridization.

Behavioural analysis

Male $Atp1a3^{+/-}$ were backcrossed for 7–12 generations and $Atp1a3^{+/-}$ and wild-type littermates (WT) were used in these studies. Mice were housed in a 12 h light/dark cycle (lights on between 07:00 and 19:00 h). All behavioural observations were made during the light phase, except for monitoring home cage activity. Room temperature was set at 23–25°C. Food and water were available *ad libitum*. Sex differences were not assessed in detail.

Measurement of spontaneous motor activity. Spontaneous motor activity in the home cage was monitored for 48 h by using the Activity Sensor Unit for mouse system (AS-TIME/Ver.1, O'Hara & Co., Tokyo, Japan), which detects heat radiation from the mouse body.

Open field test. To measure locomotor activity in the new environment, the mouse was placed in the centre of a white acrylic cage (50 × 50 × 40 cm) (O'Hara & Co.), and locomotion activity was measured automatically over a period of 10 min using NIH Image software.

Rotarod test. The apparatus consists of a bar (9 cm in diameter) with discs at both sides (Rotarod treadmill for mice, O'Hara & Co.). The bar started to rotate at a speed of 2 r.p.m., and then the rotating speed was increased by 0.15 r.p.m. s^{-1} until 20 r.p.m. (120 s) or when the mouse fell down. The integrity of motor coordination was assessed by measuring the latency to fall from the rod. Mice were habituated to the apparatus once per day for 4 days before testing and examined following three successive days (days 1, 2 and 3).

Balanced beam test. The apparatus consisted of a 1 m long bar (28 or 11 mm in diameter) with a black escape box on one end (O'Hara & Co.). Mice were acclimated to go into the escape box on the 28 mm diameter bar for 2 days before testing. The latency to reach the box on the 11 mm diameter bar was measured. Mice were examined for four successive days (days 1, 2, 3 and 4).

Intracerebellar kainate injection

These experiments were conducted in 9–14 week-old male littermates weighing approximately 25 g (weight: 26.5 ± 0.43 g for WT, $n = 16$; 25.1 ± 0.68 g for $Atp1a3^{+/-}$, $n = 15$). The mouse was intraperitoneally anaesthetized with 200 mg kg^{-1} Avertin (tribromoethanol; Sigma-Aldrich) and positioned in a stereotaxic frame equipped with a warm base. A stainless steel guide 25-gauge (G) cannula was inserted into the brain with the tip in the cerebellum and secured to the skull with screws and dental cement. The coordinate of the tip was 6.5 mm caudal to bregma, 1.5 mm lateral to the midline and 2 mm below the skull. On post-operative days 7–13, 0.5 μl of 100 μg ml^{-1} kainate (Sigma Aldrich) solution dissolved in PBS was injected into the cerebellum over 30 s via a 32-G needle connected to a 10 μl Hamilton syringe. The tip of the needle extended 2 mm beyond the guide cannula. Immediately after the injection, the mouse was placed in an empty cage and observed by video recording for 1 min every 10 min for 2 h. Scoring was performed in a blinded fashion. The disability score was evaluated during the observation period (Pizoli *et al.* 2002). Scores of D4 and D5 represent sustained dystonic posture with limited ambulation and prolonged immobility in dystonic posture, respectively (D4/D5) and evaluated as dystonic response. If no spontaneous dystonia was observed at the beginning of each 1-min recording, mice were lifted by the tail and placed down again to induce locomotion, which

often preceded dystonia. At the end of the experiments, the brain was removed from the skull and fixed in fixation solution (4% paraformaldehyde/0.1 M PBS, pH 7.4). The fixed cerebellum was sectioned and each section was stained for histological examination of the injection site.

Immunofluorescence

Mice were killed under pentobarbital anaesthesia (60–70 mg kg^{-1} somnopentyl; Kyoritsu Seiyaku, Tokyo, Japan) and transcardially perfused with fixation solution. The brain was isolated and further fixed at 4°C in fixation solution for 3–24 h, depending on the age. Samples were immersed in 18–30% sucrose/PBS, embedded in optimal cutting temperature (OCT) compound (Sakura Finetek, Torrance, CA, USA), then frozen on dry ice, and cut into 20–30 μm-thick cryosections, followed by immunofluorescence. The primary antibodies used were anti-γ-aminobutyric acid transporter (VGAT) (1:500 dilution, Frontier Inst., Ishikari, Hokkaido, Japan), anti-glutamate decarboxylase (GAD)65 and GAD67 (GAD65/67, 1:1000 dilution, Sigma), anti-vesicular glutamate transporter 1 (VGLUT1, 1:500 dilution, home-made antiserum) and VGLUT2 (1:500 dilution, home-made antiserum). Guinea-pig and rabbit anti-Na pump α3 antibody was prepared against mouse peptides, HETEDPNDNRYL (Pressley, 1992). The specificities of the above antibodies were verified by Western blotting and immunostaining using embryonic day (E)18.5 *Atp1a3*$^{-/-}$ with no positive signals. The secondary antibodies for fluorescence staining (1:1000 dilution) were anti-rabbit conjugated Cy3 (Amersham Biosciences, Piscataway, NJ, USA) and Alexa Fluor 488 anti-rabbit, Alexa Fluor 488 anti-guinea pig and Alexa Fluor 546 anti-guinea pig (Molecular Probes/Invitrogen, Carlsbad, CA, USA). 4,6-Diamidino-2-phenylindole (DAPI, Sigma) was used for nuclear staining. Images of samples were obtained with 20× or 40× objectives of an Olympus FV1000 confocal microscope (Olympus Optical, Tokyo, Japan). Experiments were performed in at least three sets of different embryos and the results were similar. Representative results are shown in the figures.

RNA probes and *in situ* hybridization

Partial cDNAs of mouse *Atp1a1* (nucleotide number 3350–3604, NM_144900), *Atp1a2* (nucleotide number 3236–3788, NM_178405) and *Atp1a3* (nucleotide number 3170–3843, NM_144921) were obtained by RT-PCR with total RNA of both mouse E15.5 embryos and mouse adult brain prepared using Isogen (Nippon Gene, Japan). They were subcloned into pGEM-T Easy Vector (Promega, Madison, WI, USA). The linearized plasmids were used for riboprobe templates. Brains were isolated as described above. *In situ* hybridization was performed on 30 μm-thick cryosections using single-stranded digoxigenin-UTP (Roche Diagnostics, Basel, Switzerland)-labelled riboprobes. Hybridization was performed at 50°C as described previously (Ikeda *et al.* 2007). Signals were detected with an anti-digoxigenin antibody conjugated to alkaline phosphatase (AP; Roche, Indianapolis, IN, USA) and nitro-blue tetrazolium/5-bromo-4-chloro-3′-indolylphosphate (NBT/BCIP; Roche) for chromogen.

Cerebellar slice preparation and electrophysiological recording

Experiments were performed as described previously (Satake *et al.* 2010). In brief, mice (11–15 days old) were deeply anaesthetized by inhalation of halothane and immediately killed by decapitation. The isolated cerebellar vermis were parasagittally sliced at 250 μm thickness using a vibratome (VT1000S; Leica, Nussloch, Germany) in an ice-cold Na^+-deficient saline that contained (in mM): sucrose, 300.0; KCl, 3.4; $CaCl_2$, 0.3; $MgCl_2$, 3.0; Hepes, 10.0; NaH_2PO_4, 0.6; and glucose, 10.0 (pH adjusted to 7.4 with NaOH, and the saline was continuously equilibrated with 100% O_2 gas). The slices were incubated at room temperature for at least 1 h in the interface of a chamber filled with 95% O_2/5% CO_2 gas and artificial cerebrospinal fluid (ACSF). The ACSF contained (in mM): NaCl, 138.6; KCl, 3.35; $CaCl_2$, 2.5; $MgCl_2$, 1.0; $NaHCO_3$, 21.0; NaH_2PO_4, 0.6; and glucose, 10.0 (the ACSF was equilibrated with O_2/CO_2 gas to maintain pH at 7.4). The slice was transferred to a recording chamber mounted on the microscope stage (BX50WI; Olympus) and continuously superfused with the ACSF. The flow rate was set at 1.0–5.0 ml min^{-1}, and all experiments were performed at room temperature.

Synaptic responses were recorded from PCs by the whole-cell voltage-clamp technique. Membrane potentials were mostly held at −30 mV using a voltage-clamp amplifier (EPC-9; HEKA Elektronik, Lambrecht, Germany) and PatchMaster software (HEKA Elektronik). The patch-clamp glass electrodes (resistance 4–6 MΩ) were filled with an internal solution that contained (in mM): Cs-methanesulfonate, 150.0; KCl, 5.0; K-EGTA, 0.1; Na-Hepes, 5.0; Mg-ATP, 3.0; and Na-GTP, 0.4 (pH adjusted to 7.4 with CsOH). Series resistance was compensated by 60%, and the current signals were filtered at 3 kHz and digitized at 20 kHz. The series resistance and leak currents were monitored continuously, and cells were discarded from further analysis when these parameters changed significantly during the recording. Membrane potentials were recorded from molecular-layer interneurons in current-clamp mode: the composition of

the internal solution was (in mM): potassium gluconate, 140.0; KCl, 5.0; K-EGTA, 0.2; $MgCl_2$, 2.0; Mg-ATP, 3.0; and Na-GTP, 0.4 (pH adjusted to 7.4 with KOH). For loose cell-attached recordings, the glass electrode was gently placed in contact with a molecular-layer interneuron and slight suction was applied (Hirono & Obata, 2006). The electrode contained ACSF and was maintained at 0 mV.

Postsynaptic currents were evoked by focal stimulation through ACSF-filled glass electrodes (strength of the stimulation current is indicated in the figure legends, single pulse for 100 μs). Excitatory postsynaptic currents (EPSCs) were recorded in the continuous presence of 100 μM picrotoxin (Sigma-Aldrich) in the external ACSF, and climbing fibre (CF)- and parallel fibre (PF)-mediated EPSCs were distinguished as described (Satake *et al.* 2000). Molecular layer (ML) interneuron-mediated inhibitory postsynaptic currents (IPSCs) were evoked by stimulation at one-quarter of the ML depth in the presence of 6-cyano-7-nitroquinoxaline-2,3-dione (CNQX; Tocris Cookson, Bristol, UK; 20 μM). Stimulus artifacts have been truncated for illustration purposes. Chemicals used in this work were as follows: tetrodotoxin (TTX, Peptide Institute Inc., Osaka, Japan); γ-D-glutamylglycine (γ-DGG, Tocris); cyclothiazide (Tocris); and (*RS*)-1-aminoindan-1,5-dicarboxylic acid (AIDA, Tocris). The effects of drugs were examined after application for at least 15 min.

Statistical analysis

Data are expressed as mean ± SEM. Differences between groups were examined for statistical significance using one- or two-way analyses of variance (ANOVAs) and *post hoc* multiple comparison tests in electrophysiological experiments, and Student's *t* test in behavioural analyses. Differences with P values of < 0.05 were considered statistically significant.

Results

Construction of *Atp1a3*-deficient mice and behavioural analyses

We constructed and prepared the knockout mouse line *Atp1a3* (Fig. 1). Mice homozygous for the *Atp1a3* deletion mutation ($Atp1a3^{-/-}$) died just after birth due to complete lack of breathing movements (K. Ikeda & H. Onimaru, unpubl. data). Because haploinsufficiency of *ATP1A3* ($ATP1A3^{+/-}$) is thought to contribute to RDP, we compared heterozygous mice ($Atp1a3^{+/-}$) with their wild-type littermates (WT). $Atp1a3^{+/-}$ showed no gross morphological defects, no apparent histological anomalies in the brain and survived as WT. Adult $Atp1a3^{+/-}$ were hyperactive (increased locomotor activity) in both the home cage and the open field, compared with WT (Table 1 and Fig. 2*A*; Moseley *et al.* 2007; DeAndrade *et al.* 2011). The time spent in the centre area of the open field was not different between $Atp1a3^{+/-}$ and WT (Fig. 2*B*), suggesting that there was no difference in anxiety behaviour between the two. The $Atp1a3^{+/-}$ also showed enhanced performances on the rotarod test (Fig. 2*C*) and balanced beam paradigm (Fig. 2*D*) compared with WT. Although relevance to the clinical symptoms is not clear, the observation of a better sense of motor balance in $Atp1a3^{+/-}$ motivated us to analyse altered cerebellar function.

Table 1. Spontaneous motor activity in the home cage of the adult wild-type and $Atp1a3^{+/-}$ littermates for 48 h

	Spontaneous activity (counts day^{-1})		
Atp1a3 genotype	Total	Dark	Light
Wild-type	16413 ± 1304	14729 ± 1125	1548 ± 215
$Atp1a3^{+/-}$	24614 ± 3326	21038 ± 2811	3577 ± 551

There is a significant difference between the wild-type ($n = 8$) and the heterozygous $Atp1a3^{+/-}$ mice ($n = 7$) at total ($P = 0.031$), dark ($P = 0.047$) and light ($P = 0.003$) phases ($P < 0.05$). Ten- to 12-week-old mice were analysed.

Induction of dystonia by intracerebellar injection of kainate

$Atp1a3^{+/-}$ did not develop dystonia either spontaneously under normal environment or after various mild behavioural stimuli, such as suspension by the tail (each mouse was suspended by its tail for 15 min) and forced swimming, or restraint stress (data not shown). We hypothesized that one of the reasons for the lack of manifestation of symptoms was inadequate developmental changes in the synaptic circuits by the above mild and transient stresses in $Atp1a3^{+/-}$. Therefore, dystonia was induced by pharmacological disturbance of synaptic circuit. To specify the primary focal region of dystonia, we used microinjection of low doses of kainate, an excitatory glutamate agonist, directly into the cerebellar vermis. This experimental approach was based on a previous well-described refined procedure that induces abrupt disruption of synaptic transmission in the cerebellum with resultant dystonia phenotype (Pizoli *et al.* 2002). Following injection of kainate into the cerebellum, the duration of sustained dystonic response was measured over 1 min every 10 min until 2 h after injection. The first sign of dystonia appeared 10–20 min after the injection in both WT and $Atp1a3^{+/-}$. A typical dystonic response encompassed persistent hold up of the hindlimb against the trunk. Furthermore, intentional movements often

induced dystonic posture in both WT and *Atp1a3*$^{+/-}$. The total time of sustained dystonic response (score D4/D5 in Pizoli *et al.* 2002) was longer in *Atp1a3*$^{+/-}$ than in WT (Fig. 2*E*). Furthermore, recovery from the effect of kainate injection (i.e. disappearance of dystonia) was significantly later in *Atp1a3*$^{+/-}$ than in WT (Fig. 2*F*). In addition, the mean D4/D5 response (number of events) was significantly larger in *Atp1a3*$^{+/-}$ than in WT (Fig. S1*A*). However, the mean duration of individual events was not different between *Atp1a3*$^{+/-}$ and WT (Fig. S1*B*). The position of the microinjection site was not different between the two groups (data not shown), indicating that the increased response in *Atp1a3*$^{+/-}$ was not due to differences in the site of kainate injection in the cerebellum.

Expression of *Atp1a3* in the cerebellum

The distribution of Na pump α3 protein in the brain of 3-month-old (adult) mice was investigated recently by immunohistochemistry (Bøttger *et al.* 2011). In the present study, we confirmed the mRNA expression of *Atp1a1*, *Atp1a2* and *Atp1a3* in the cerebella at younger ages [postnatal days (P) 35–40]. The expression of each α subunit gene showed a distinct pattern (Fig. 3). *Atp1a1* transcript was observed in the granular layer (GL), while *Atp1a2* was noted mainly in the Purkinje cell layer (PCL), with scattered signal in the GL and white matter (WM) of the cerebellum, and in the pia mater (arrowhead in Fig. 3*D*), as reported previously (Moseley *et al.* 2003). *Atp1a3* showed unique expression patterns: it was observed in the cell bodies in PCL, throughout the ML,

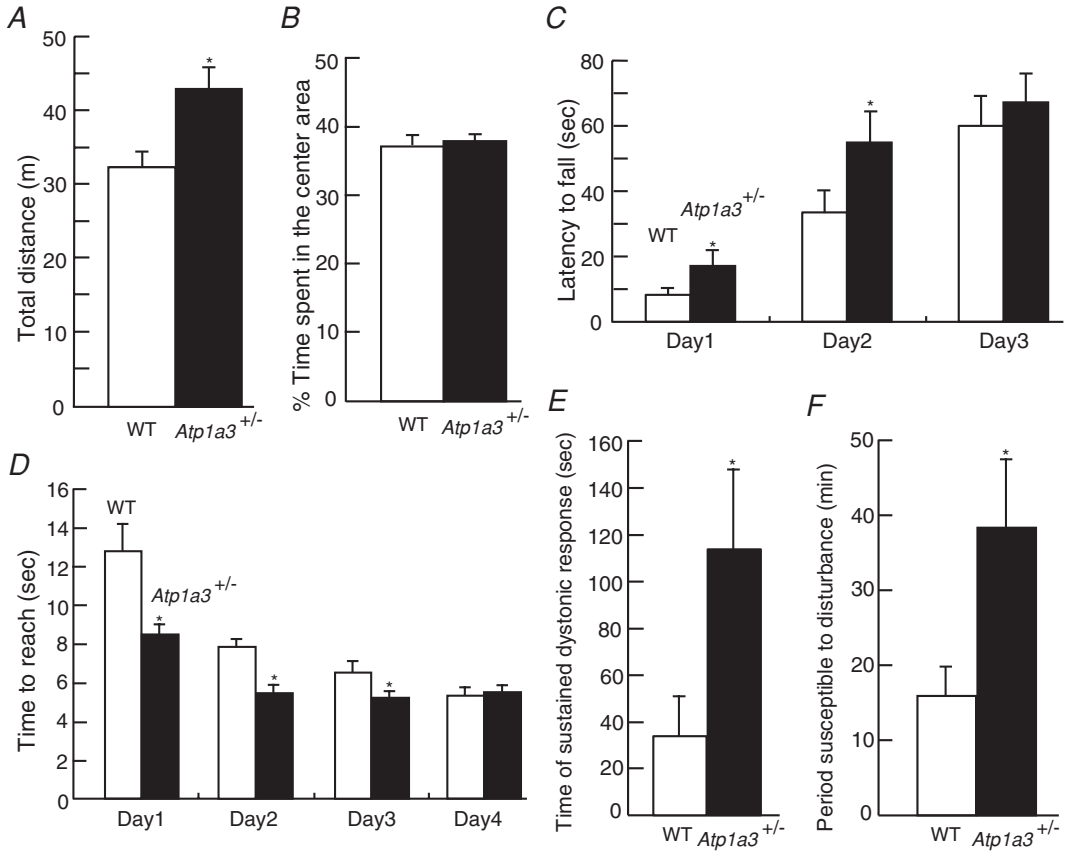

Figure 2. Altered behaviours in *Atp1a3* heterozygous mice (*Atp1a3*$^{+/-}$)
A and *B*, open field test (10 week-old mice); $n = 12$ for each male genotype mouse. *A*, total path length in the open-field test. *Atp1a3*$^{+/-}$ showed significantly increased activities compared with wild-type littermates (WT). *B*, percentage of time spent in the centre area. *C*, rotarod test (3 week-old female mice); $n = 18$ for WT and $n = 19$ for *Atp1a3*$^{+/-}$. Latency to fall from the rod was measured. *Atp1a3*$^{+/-}$ showed significantly better performance than WT at days 1 and 2. No significant difference was observed on day 3. *D*, balanced beam test (11–14 week-old mice); $n = 12$ for each male genotype mouse. Time to reach an escape box was measured. Performance on days 1–3, but not day 4, was significantly better in *Atp1a3*$^{+/-}$ than WT. *E*, duration of sustained dystonic response (score D4/D5, Pizoli *et al.* 2002). *Atp1a3*$^{+/-}$ showed significantly increased time during which dystonic responses were observed. *F*, susceptible time of dystonia induction to disturbance. *Atp1a3*$^{+/-}$ showed significantly longer sensitivity to induced dystonic response; $n = 16$ (WT) and $n = 15$ (*Atp1a3*$^{+/-}$). Data are mean ± SEM. Open bars: WT, filled bars: *Atp1a3*$^{+/-}$. $^*P < 0.05$.

especially in interneurons, basket and stellate cells, and also in Golgi cells of the GL, but not in granule cells, indicating that *Atp1a3* is expressed in GABAergic neurons. High levels of *Atp1a3* transcripts were also observed in neurons of the cerebellar nuclei (CN), which are projected by GABAergic inhibitory synapses from PCs. Our results add support to previous findings of *Atp1a3* mRNA expression in GABAergic neurons, namely PCs, basket and stellate cells in ML, as well as Golgi cells in GL of juvenile rodents (Hieber *et al.* 1989, 1991; Chauhan & Siegel, 1997).

We further examined the expression of *Atp1a3* in the developing pup (P14), because dystonia symptoms in RDP patients most commonly appear in young age (Brashear *et al.* 2008). In the cerebellum, the expression level and pattern of *Atp1a3* were essentially similar to those at P40 (data not shown). *Atp1a3* was highly expressed in the subthalamic nucleus and substantia nigra, moderately expressed in the globus pallidus and less abundantly expressed in the caudate putamen, which are considered primary causal regions of dystonia.

Localization of the Na pump α3 subunit in the cerebellum

Immunostaining of the α3 subunit was observed as dots in the ML and on the surface of PC soma (Fig. 4*B* and *F*). The presynaptic marker of GABAergic neurons, VGAT, was positive, showing a dotted appearance on the membrane of PC bodies and dendrites, and those signals mostly overlapped with that of the α3 subunit (Fig. 4*E–H*), indicating accumulation of the α3 subunit in the inhibitory synapses. Moreover, excess staining for the α3 subunit was noted in the cerebellar pinceaux, together with VGAT (Fig. 4*D* and *H*). The pinceaux is a thick cup-like structure inferior

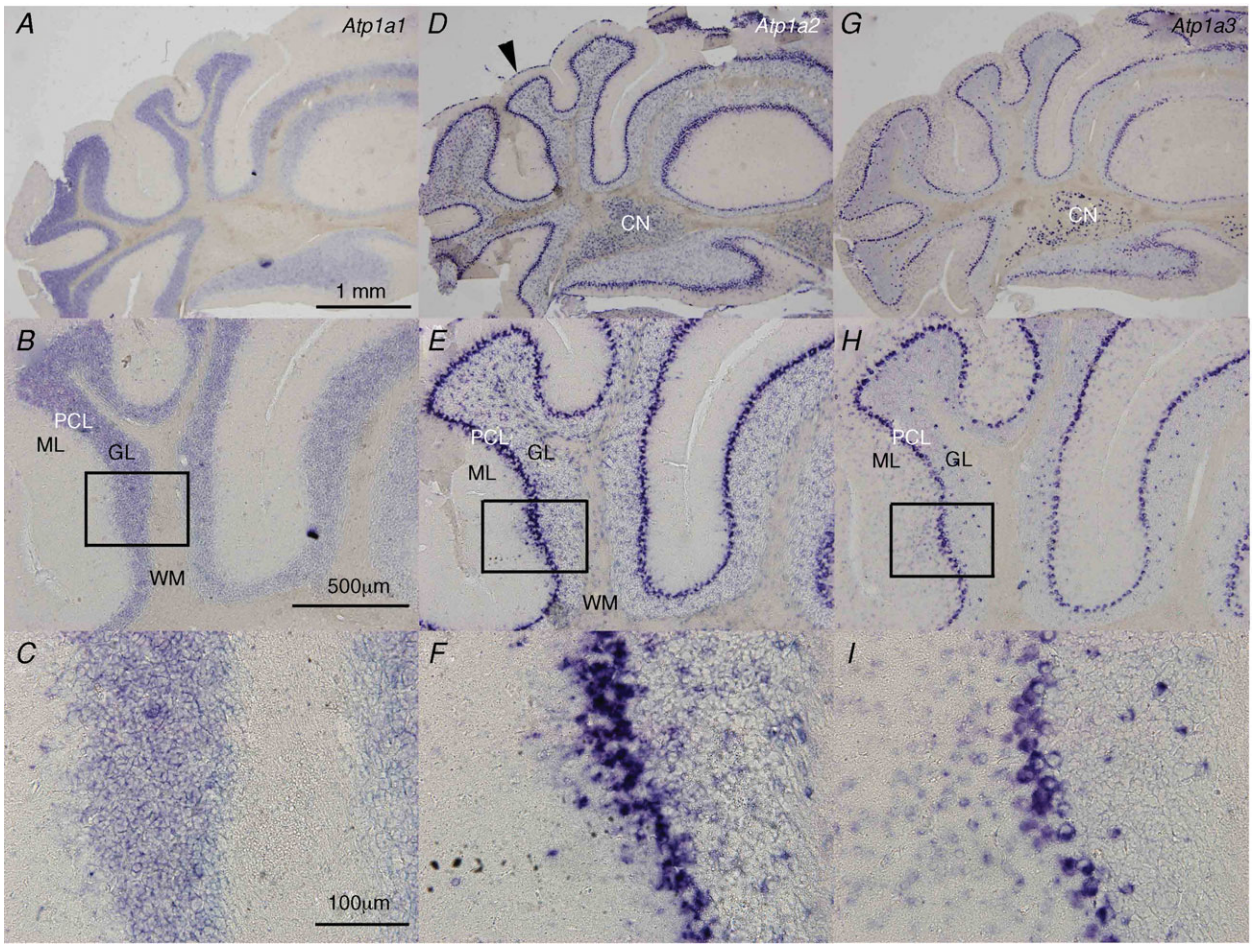

Figure 3. mRNA expression of Na pump α subunits in the cerebellum of juvenile mouse (postnatal day 40)
Alternate sections were examined by *in situ* hybridization using different probes. *A–C*, *Atp1a1* mRNA expression. *D–F*, *Atp1a2* mRNA expression. *Atp1a2* mRNA expression in the pia matter (arrowhead). *G–I*, *Atp1a3* mRNA expression. Boxes in *B*, *E* and *H* show areas that are pictured beneath at higher magnifications (*C*, *F* and *I*, respectively). In each panel, the top is the dorsal and the right is the medial side. CN, cerebellar nuclei; ML, molecular layer; GL, granular layer; PCL, Purkinje cell layer; WM, white matter.

to the PC somata and dense terminal plexus around the axon hillock and initial segment of PC. It is formed by convergence of axonal collaterals descending from ML basket cells and stellate cells, and is highly immunopositive for VGAT (Takayama & Inoue, 2004; Sotelo, 2008). The α3 subunit was also co-immunostained with GAD65/67, which were expressed in most GABA-containing neurons (Fig. 4*I*). The α3 subunit was co-localized with excitatory presynaptic markers, VGLUT1 and VGLUT2, in the mossy fibre-granule cell synapses in GL (Fig. 4*J* and *K*), but not in PCs (Fig. 4*J* and *K*). These results indicate the expression of *Atp1a3* in inhibitory neurons and high accumulation of its products in inhibitory terminals and pinceaux.

Characterization of neurotransmission from ML interneurons to PCs

The above results showed increased response to dystonia induction by kainate injection into the cerebellum of *Atp1a3*$^{+/-}$ and strong expression of *Atp1a3* in inhibitory neurons in the developing cerebellum. The inhibitory microcircuitry of the cerebellar cortex has been thought to play a key role in orchestrating synaptic integration and precise timing of action potentials in PCs, the sole output neuron from the cerebellum (for a review, see Jörntell *et al.* 2010). Taken together, it is likely that disturbance of the inhibitory synaptic transmission onto PCs could occur in *Atp1a3*$^{+/-}$. Accordingly, we compared the properties of GABAergic neurotransmission from ML interneurons to PCs between WT and *Atp1a3*$^{+/-}$ using the whole-cell voltage-clamp technique.

IPSCs were recorded from visually identified PCs of cerebellar slices prepared from young pup littermates (P12–15, $V_H = -30$ mV), and stimulation electrodes were placed in the inner fourth of the ML to activate axons of ML interneurons (thus, they were mostly basket cells). When stimulation intensity was increased from 10 to 100 μA, the amplitude of IPSCs increased almost

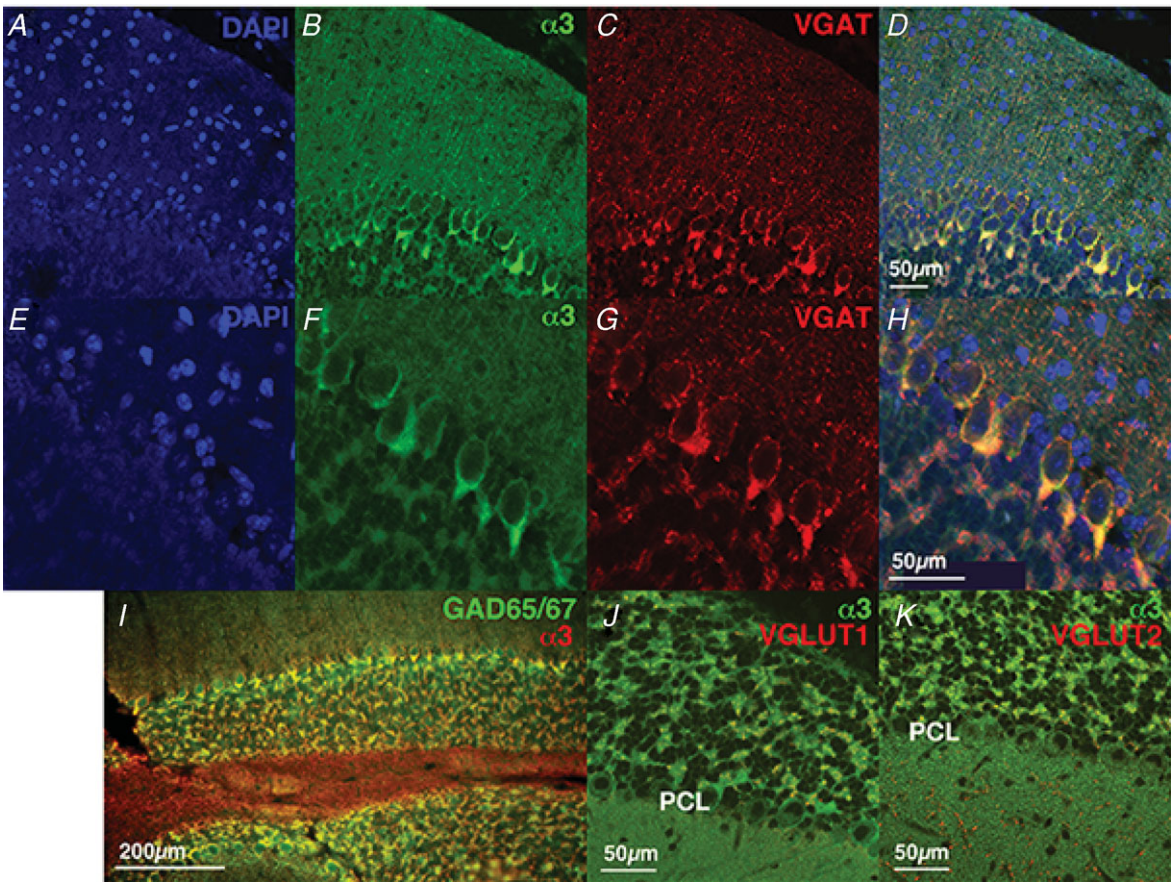

Figure 4. Expression of Na pump α3 subunits, VGAT, GAD65/67, VGLUT1 and VGLUT2 in the cerebellum of young wild-type mice
Immunofluorescence using antibodies to α3 (green, *B* and *F*) and VGAT (red, *C* and *G*). Nuclei are stained with DAPI (blue, *A* and *E*). *E*–*H*, higher magnifications of *A*–*D*. Merged figures of α3 and VGAT are shown in *D* and *H*. A merged figure of immunofluorescence using antibodies to α3 (red) and GAD65/67 (green) is shown in *I*. Merged figures using antibodies to α3 (green) and VGLUT1 (red, *J*) or VGLUT2 (red, *K*) are shown. *A*–*I*, P26 mice; *J* and *K*, P39 mice.

linearly in both *Atp1a3*$^{+/-}$ and WT (Fig. 5*A* and *B*). The effect of stimulation in eliciting IPSCs appeared to be consistently stronger in PCs of *Atp1a3*$^{+/-}$ (solid triangles) than WT (open circles), although the difference was not statistically significant ($F_{1,231} = 1.65$, $P = 0.20$, two-way ANOVA). A further increase in the stimulation intensity to 300–500 μA increased the amplitude of IPSCs to a similar plateau level in both WT and *Atp1a3*$^{+/-}$; the mean IPSC amplitude at 500 μA was not different between WT and *Atp1a3*$^{+/-}$ (1026 ± 223 pA, $n = 12$ and 970 ± 226 pA, $n = 11$, respectively, $P = 0.86$, Fig. 5*A* and *B*). This suggests that the majority of ML interneuron axons present in the activation field were stimulated by the saturated intensity (namely, 300–500 μA). Comparison of the relationship between IPSC amplitude and stimulation intensity after normalization of the amplitude by the amplitude of IPSCs evoked at a stimulation intensity of 500 μA (Fig. 5*C*) showed a significant leftward shift in the relationship in *Atp1a3*$^{+/-}$ ($F_{1,219} = 15.6$, $P < 0.001$). This suggests a decreased threshold of ML interneuron response to electrical stimulation in *Atp1a3*$^{+/-}$. To get insight into the mechanism underlying the enhancement of cerebellar inhibitory neurotransmission in *Atp1a3*$^{+/-}$, we applied a pair of stimulation pulses at varying intervals, and compared the paired-pulse ratio (PPR) of the amplitude, i.e. the second IPSC amplitude/the first IPSC amplitude (Fig. 5*D*; Satake *et al.* 2000; Zucker & Regehr, 2002). As shown in Fig. 5*D* and *E*, the PPR of IPSCs was not significantly different between WT and *Atp1a3*$^{+/-}$ at any tested intervals ($F_{1,175} = 0.061$, $P = 0.81$).

At young age, the mouse cerebellar inhibitory neurotransmission between ML interneurons and PCs shows remarkable paired-pulse depression (Fig. 5*D* and *E*; for further details, see Pouzat & Hestrin 1997). Because the PPR appears to be less sensitive to presynaptic potentiation at the high release probability synapse, for example, compared with the frequency of miniature IPSC (mIPSC) (Mitoma & Konishi, 1999; Saitow *et al.* 2000), we next recorded mIPSCs in PCs in the presence of 1 μM TTX, and compared their frequency and amplitude between WT and *Atp1a3*$^{+/-}$. The frequency of mIPSCs was much higher in *Atp1a3*$^{+/-}$ than in WT (Fig. 6*A*, *B* and *D*, $P = 0.034$). In contrast, the amplitude distribution of mIPSCs was similar (Fig. 6*C*) and the mean amplitude was not different

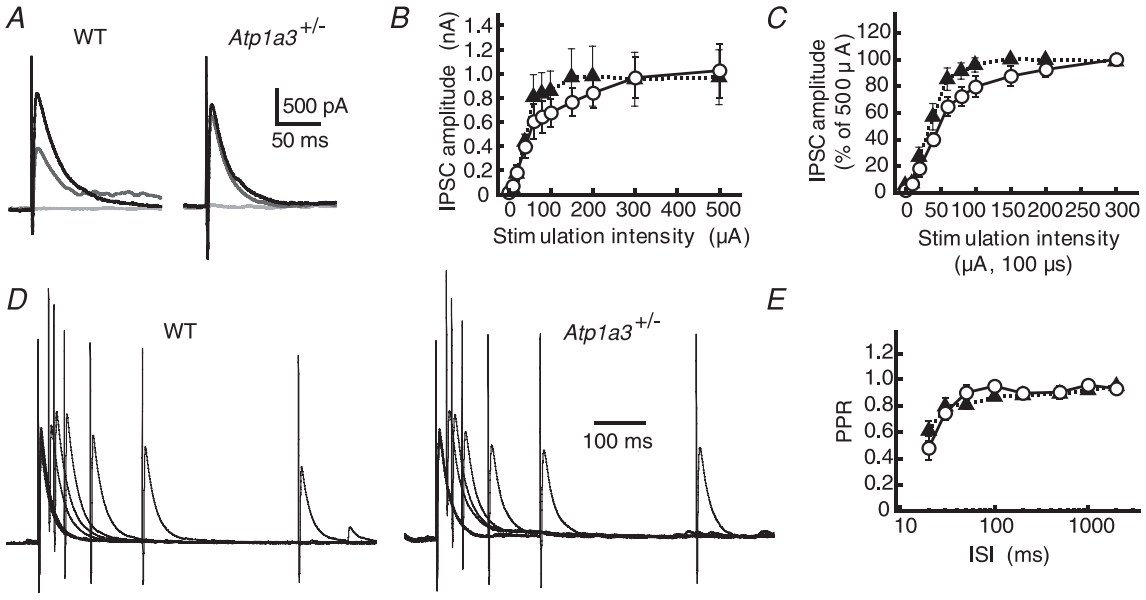

Figure 5. Comparison of ML interneuron-mediated inhibitory neurotransmission onto Purkinje cells (PCs) between WT and *Atp1a3*$^{+/-}$

A, representative traces of IPSCs recorded from a single PC of WT and *Atp1a3*$^{+/-}$. The IPSCs were evoked by electrical stimulation with a series of different intensity (from 10 to 500 μA for 100 μs), and superimposed for stimulations at 10 (pale grey lines), 60 (dark grey lines) and 500 μA (black lines). Each trace is derived from averaging the IPSCs of several successive traces recorded every 15 s. Stimulation artifacts were truncated for clarity. *B*, relationship between IPSC amplitude and stimulation intensity for WT (open circles, $n = 12$) and *Atp1a3*$^{+/-}$ (filled triangles, $n = 11$). Data are mean ± SEM. *C*, relationship between IPSC amplitude and stimulation intensity of WT (open circles, $n = 12$) and *Atp1a3*$^{+/-}$ (filled triangles, $n = 11$). Data are relative to the amplitude examined at stimulation intensity of 500 μA. Note the significantly higher response to the weak stimulation intensity in *Atp1a3*$^{+/-}$. *D*, representative averaged traces of IPSCs examined by the paired-pulse protocol in PCs of WT and *Atp1a3*$^{+/-}$. The traces were normalized relative to the peaks of the first IPSC. *E*, relationship between the paired-pulse ratio (PPR) and the inter-stimulus intervals (ISI) for IPSCs examined in WT (open circles, $n = 11$) and *Atp1a3*$^{+/-}$ (filled triangles, $n = 12$).

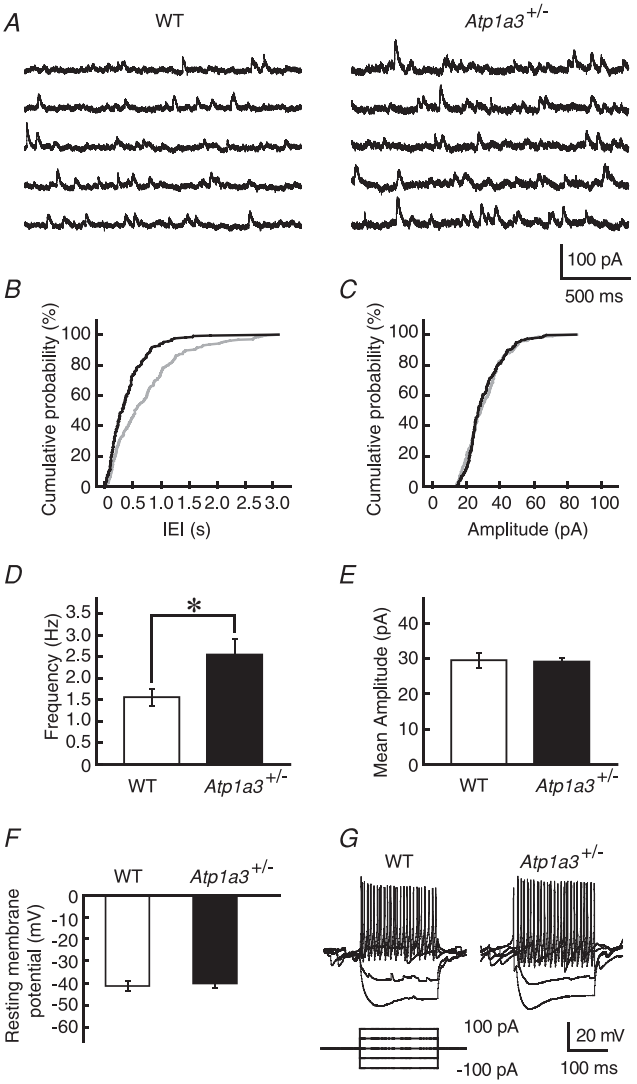

Figure 6. Characterization of miniature IPSCs (mIPSCs) in *Atp1a3*$^{+/-}$ compared with WT
A, successive traces of mIPSCs recorded from single PCs of WT and *Atp1a3*$^{+/-}$ in the continuous presence of TTX (1 μM) and CNQX (20 μM). *B* and *C*, cumulative distribution of the inter-event intervals (IEI in *B*) and amplitude of mIPSCs (*C*) of WT (grey lines) and *Atp1a3*$^{+/-}$ (black lines). Data were calculated from the trace in *A*. Note the significant leftward shift in the IEI distribution in the *Atp1a3*$^{+/-}$ ($P < 0.001$, Kolmogorov–Smirnov test in *B*) without a change in the amplitude distribution ($P = 0.33$, Kolmogorov–Smirnov test in *C*). *D* and *E*, comparison of the frequency (*D*) and mean amplitude (*E*) between mIPSCs recorded from PCs of WT (open bar, $n = 13$) and *Atp1a3*$^{+/-}$ (filled bar, $n = 12$). *F*, comparison of the resting membrane potential of ML interneurons between WT (open bar and circles, $n = 12$) and *Atp1a3*$^{+/-}$ (filled bar and triangles, $n = 11$) ($P = 0.46$, unpaired *t* test). *G*, representative traces of voltage responses recorded from single ML interneurons from WT and *Atp1a3*$^{+/-}$. Each trace is derived from several successive traces recorded by the current-clamp technique. Current injection protocol is shown under the trace. Data are mean ± SEM. *$P < 0.05$.

between WT and *Atp1a3*$^{+/-}$ ($P = 0.84$, Fig. 6*E*). These results suggest that the properties of the postsynaptic GABA receptor do not seem to be significantly different between WT and *Atp1a3*$^{+/-}$, but rather that enhancement of GABAergic transmission in *Atp1a3*$^{+/-}$ originates in a presynaptic mechanism. The latter agrees with the presynaptic expression of *Atp1a3* in ML interneurons (Fig. 3). We further examined the resting membrane potentials (E_m) of ML interneurons in the current-clamp mode, assuming that reduced expression of α3 subunits leads to membrane depolarization and thereby increases the excitability of ML interneurons. The E_m was examined in the presence of 1 μM TTX; E_m was -41.3 ± 2.5 mV in WT ($n = 12$) and -40.1 ± 2.1 mV in *Atp1a3*$^{+/-}$ ($n = 11$), and the difference was not statistically significant ($P = 0.72$, Fig. 6*F*). We also compared the excitability of ML interneurons between WT and *Atp1a3*$^{+/-}$ by injecting square wave currents from the recording pipette, but did not find any remarkable difference in the response (Fig. 6*G*). Furthermore, comparison of the spontaneous firing rate of interneurons by loose cell-attached recordings showed no significant difference between WT (4.6 ± 1.6 Hz, $n = 15$) and *Atp1a3*$^{+/-}$ (5.2 ± 1.2 Hz, $n = 10$) ($P = 0.77$, Fig. S2). These results rule out the possibility that the enhancement of cerebellar GABAergic neurotransmission in *Atp1a3*$^{+/-}$ is due to increased somatic excitability of ML interneurons. Together with the presynaptic accumulation of α3 subunit immunoreactivity in ML interneurons (Fig. 4), it is likely that the increase in inhibitory neurotransmission in *Atp1a3*$^{+/-}$ originates in axonal, but not somatic, depolarization of the interneuron.

Properties of PF- and CF-PC synapses

Next, we compared the properties of the excitatory synaptic transmission from PFs or CFs to PCs between WT and *Atp1a3*$^{+/-}$ at P12–15 ($V_H = -60$ mV or -30 mV, respectively). The amplitudes of PF-mediated EPSCs increased almost linearly depending on the increment in stimulation intensity in WT and *Atp1a3*$^{+/-}$ (Fig. 7*A*). Stimulation with a higher intensity (300–500 μA) increased the amplitude of EPSCs to a plateau level and the mean amplitude at 500 μA was not significantly different between WT and *Atp1a3*$^{+/-}$ (1.35 ± 0.26 nA, $n = 11$ and 1.54 ± 0.34 nA, $n = 11$, respectively; $P = 0.66$). There was also no significant difference between WT and *Atp1a3*$^{+/-}$ even when the relationship between stimulation intensity and EPSC amplitude was examined after normalization by the amplitude of EPSCs evoked at 500 μA ($F_{1,259} = 0.087$, $P = 0.77$, Fig. 7*B*). Application of a mixture of 2 mM γ-DGG, a low-affinity competitive antagonist of AMPA receptors (Wadiche & Jahr, 2001; Kodama *et al.* 2006), and 50 μM cyclothiazide, a blocker of AMPA receptor desensitization (Partin *et al.* 1993), reduced the amplitude

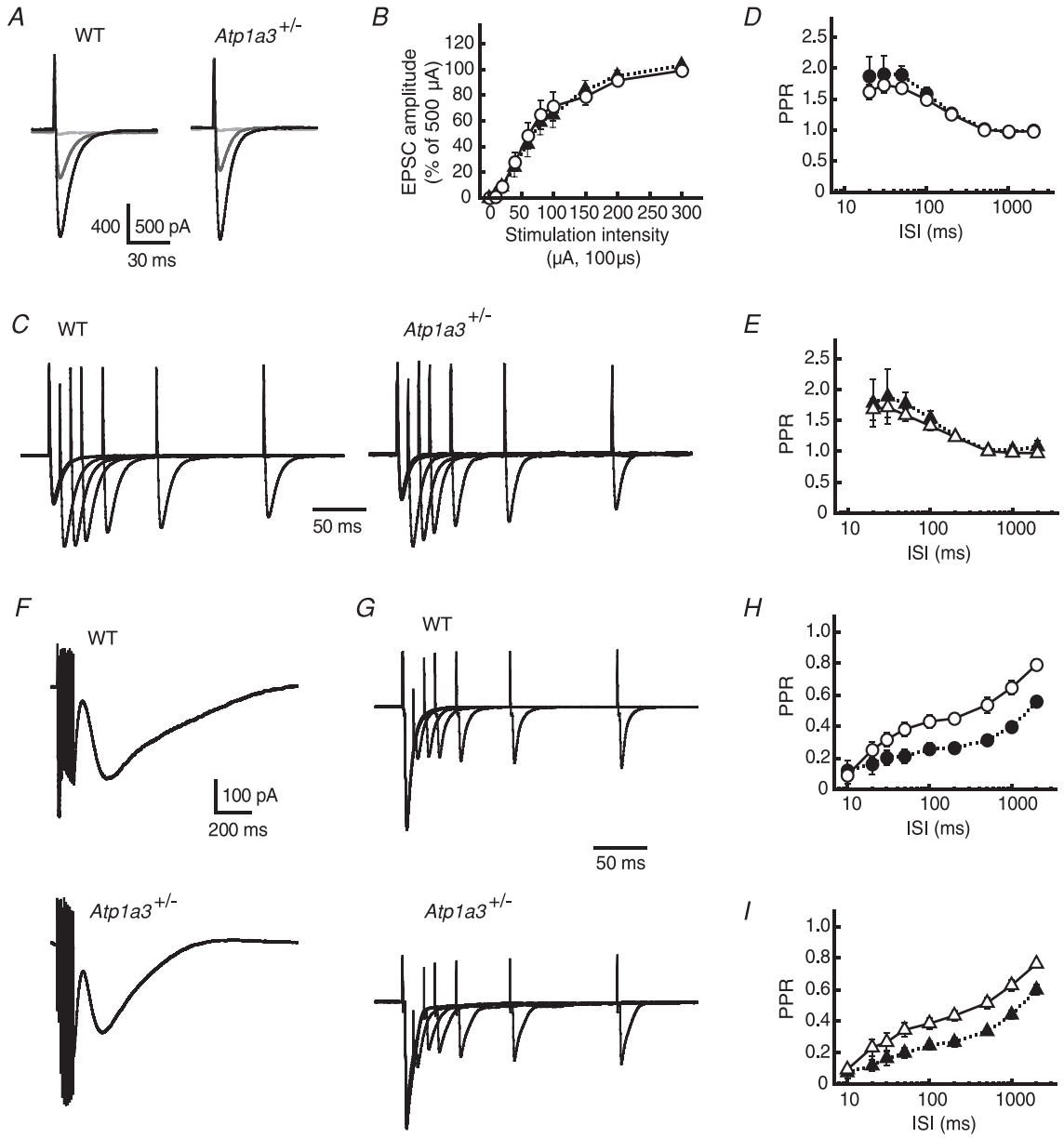

Figure 7. Comparison of parallel fibre (PF)- and climbing fibre (CF)-mediated excitatory neurotransmission onto PCs between WT and *Atp1a3*$^{+/-}$

A, representative averaged traces of PF-mediated EPSCs recorded from a single PC of WT and *Atp1a3*$^{+/-}$. The EPSCs were evoked by electrical stimulation with a series of different intensity (from 10 to 500 μA for 100 μs), and superimposed for stimulations at 10 (pale grey lines), 60 (dark grey lines) and 500 μA (black lines). Each trace is derived from averaging the EPSCs of several successive traces recorded every 15 s. Stimulation artifacts were truncated for clarity. *B*, relationship between the amplitude of PF-PC EPSCs and stimulation intensity for WT (open circles, $n = 14$) and *Atp1a3*$^{+/-}$ (filled triangles, $n = 13$). Data are mean ± SEM and are relative to the amplitude examined at a stimulation intensity of 500 μA. *C*, representative averaged traces of PF-PC EPSCs examined by the paired-pulse protocol in PCs of WT and *Atp1a3*$^{+/-}$. The traces were normalized relative to the peaks of the first EPSC. *D* and *E*, relationship between the PPR and ISI for PF-PC EPSCs examined in WT (*D*, circles) and *Atp1a3*$^{+/-}$ (*E*, triangles). The magnitudes of PPR of the EPSC were not significantly different between WT and *Atp1a3*$^{+/-}$ at any interval tested in the absence (open symbols) and presence (filled symbols) of 2 mM γ-DGG and 50 μM cyclothiazide. *F*, representative averaged traces of mGluR1/TRPC1-mediated inward currents examined in PCs of WT and *Atp1a3*$^{+/-}$. The currents were evoked by trains of PF stimuli (100 Hz for 100 ms) in the presence of 20 μM CNQX and 100 μM picrotoxin. *G*, representative averaged traces of CF-EPSCs examined by the paired-pulse protocol in PCs of WT and *Atp1a3*$^{+/-}$. The traces were normalized relative to the peaks of the first EPSC. *H* and *I*, relationship between the PPR and ISI for CF-PC EPSCs examined in WT (*H*, circles) and *Atp1a3*$^{+/-}$ (*I*, triangles). The PPR of CF-EPSCs was not different between WT and *Atp1a3*$^{+/-}$, when they were compared in the absence (open symbols) and presence (filled symbols) of γ-DGG and cyclothiazide.

of PF-EPSCs to almost the same level in WT and *Atp1a3*$^{+/-}$ (51.4 ± 6.0%, $n = 10$ and 57.8 ± 3.5%, $n = 7$, respectively; $P = 0.66$, data not shown). These results suggest that the concentration of PF transmitter in the synaptic clefts is similar between WT and *Atp1a3*$^{+/-}$ during the single EPSC. PF-EPSCs are known to exhibit a prominent paired-pulse facilitation (Fig. 7*C*). The magnitudes of the PPR of PF-EPSCs were not significantly different between WT and *Atp1a3*$^{+/-}$ at any intervals tested in either the absence ($F_{1,202} = 0.24$, $P = 0.62$) or the presence ($F_{1,128} = 0.49$, $P = 0.49$) of γ-DGG and cyclothiazide (Fig. 7*D* and *E*).

The metabotropic glutamate receptor mGluR1 in PCs plays an important role in mediating synapse formation, synaptic plasticity (long-term depression) and motor coordination (Ichise *et al.* 2000). Repetitive activation of PFs elicits mGluR1-mediated slow inward currents in PCs (Batchelor *et al.* 1994; Hirono *et al.* 1998), and a recent study indicates that this inward current is mediated by the cation channel TRPC1 (Kim *et al.* 2003). The amplitude of the mGluR1/TRPC1-mediated currents was closely dependent on the expression level of neuronal glutamate transporter EAAT4 (Wadiche & Jahr, 2005), which is specifically expressed in PCs, and their glutamate uptake capacity is highly coupled with Na pump activity of the PC. Assuming that deficient Na pump activity causes a reduction of glutamate uptake, thereby leading to enhanced activation of the perisynaptic mGluR1 in PCs, we compared the mGluR1/TRPC1-mediated currents between WT and *Atp1a3*$^{+/-}$. The mGluR1/TRPC1 currents were evoked by trains of PF stimulation (100 Hz for 100 ms) and recorded from PCs in lobule III, where the EAAT4 expression level in PCs is low (Wadiche & Jahr, 2005; Satake *et al.* 2010), in the presence of 20 μM CNQX and 100 μM picrotoxin. The amplitude of the mGluR1/TRPC1 current of *Atp1a3*$^{+/-}$ (195.9 ± 32.1 pA, $n = 19$) appeared to be slightly smaller than that of WT (220.6 ± 57.9 pA, $n = 16$), although the difference was not different statistically ($P = 0.71$, Fig. 7*F*). The currents were similarly suppressed by the mGluR1 antagonist AIDA (0.3 mM); the amplitude reached 68.9 ± 7.0% of control in WT ($n = 8$) and 60.7 ± 7.3% in *Atp1a3*$^{+/-}$ ($n = 10$) ($P = 0.44$, data not shown). These results indicate that the properties of PF-PC excitatory neurotransmission, which includes not only ionotropic receptor-mediated fast synaptic transmission but also metabotropic receptor-mediated slow perisynaptic transmission, are similar between WT and *Atp1a3*$^{+/-}$.

At early postnatal stages, most PCs are innervated by multiple numbers of olivocerebellar CFs. Then, by the end of the third postnatal week, the supernumerary CFs are eliminated until each PC is innervated by a single CF (for a review, see Watanabe & Kano, 2011). Therefore, more than one discrete CF-EPSC can be evoked in some PCs in young animals if the intensity of CF stimulation increases. We next compared properties of the single CF-mediated (namely, mature CF-mediated) EPSCs, all of which were corroborated by observing whether the EPSC is evoked in an all-or-none fashion (Kodama *et al.* 2006). As shown in Fig. 7*G*, we did not find any significant differences in their amplitudes between WT and *Atp1a3*$^{+/-}$ (3.82 ± 0.53 nA, $n = 9$ and 3.58 ± 0.64 nA, $n = 7$, respectively; $P = 0.78$, Fig. 7*H* and *I*). The amplitudes of CF-EPSCs observed in WT and *Atp1a3*$^{+/-}$ decreased similarly after application of 2 mM γ-DGG and 50 μM cyclothiazide (51.0 ± 4.9%, $n = 9$ and 51.7 ± 5.8%, $n = 6$, respectively; $P = 0.93$, data not shown), suggesting that the concentration of CF transmitter in the synaptic clefts is similar during the single EPSC. Furthermore, the PPR of CF-EPSCs was not statistically different between WT and *Atp1a3*$^{+/-}$, both in the absence ($F_{1,143} = 1.60$, $P = 0.21$) and in the presence ($F_{1,134} = 0.062$, $P = 0.80$) of γ-DGG and cyclothiazide (Fig. 7*G*–*I*).

The above results suggest that excitatory synaptic transmission converging onto PCs is not disturbed in *Atp1a3*$^{+/-}$, which is in sharp contrast to the enhanced inhibitory synaptic transmission.

Discussion

Enhanced inhibitory synaptic transmission in cerebellum of *Atp1a3*$^{+/-}$

We observed enhancement of IPSCs evoked by weak focal stimulation and increase in the frequency, but not the amplitude, of mIPSCs in PCs of *Atp1a3*$^{+/-}$ (Figs 5 and 6). These results indicate altered properties of ML interneurons in *Atp1a3*$^{+/-}$, which is explained by: (1) increased GABA release at a single axon terminal of ML interneurons and/or (2) presence of a larger number of inhibitory synapses between ML interneurons and PCs in *Atp1a3*$^{+/-}$. However, the second possibility is less likely, because ML interneuron axons present in the activation field were similarly activated by the saturated intensity between WT and *Atp1a3*$^{+/-}$ (Fig. 5). The increased GABA release in *Atp1a3*$^{+/-}$ could be explained by: (1) local (e.g. axon terminal), but not somatic, depolarization of the GABAergic ML interneuron of *Atp1a3*$^{+/-}$ that results in higher intracellular Ca^{2+} concentration (see below); (2) increased number of docked vesicles in *Atp1a3*$^{+/-}$; and/or (3) different spatial organization of the inhibitory synapse in the ML (e.g. ML interneuron – PC synaptic connections are more abundantly distributed in the internal part of the ML than in the external part). The first possibility agrees well with the present results of double immunofluorescence staining showing a profound α3 subunit accumulation in the ML interneuron terminals (Fig. 4) and interneuronal recording showing no significant somatic depolarization (Fig. 6). In

contrast, the latter two possibilities are less likely, because no significant histological differences were detected in the cerebella of WT and *Atp1a3*$^{+/-}$ so far examined (K. Ikeda, unpublished results). Further electron microscopic analysis and definitive characterization are necessary for confirmation.

Neuronal cell excitation is associated with a marked increase in intracellular Na^+ concentration ($[Na^+]_i$). Intracellular Na^+ is pumped out by the Na pump, which is followed by an immediate return of the membrane potential to resting levels. Therefore, any reduction in Na^+ affinity of the pump by mutation (see Introduction) or decrease in the number of pump molecules (i.e. haploinsufficiency) should lead to delayed recovery from high $[Na^+]_i$ after excitation of neuronal cells. Persistently high $[Na^+]_i$ prevents proper function of various transporters driven by Na^+ electrochemical gradient force. In this context, the rate of excretion of $[Ca^{2+}]_i$ through the Na^+/Ca^{2+} exchanger system should become lower in *Atp1a3*$^{+/-}$, resulting in high $[Ca^{2+}]_i$ in the axon terminals of *Atp1a3*$^{+/-}$ ML interneurons with excessive neurotransmitter release and thereby enhanced frequency of the mIPSCs in PCs. Impairment of Na^+-coupled neuronal uptake of other neurotransmitters, such as dopamine, glutamate and GABA, is also possible in *Atp1a3*$^{+/-}$, leading to excessive neurotransmitters in the extracellular space, as in the case of *Atp1a2*$^{-/-}$ (Ikeda *et al.* 2003). Indeed, the presence of extracellular GABA in the young cerebellum is known to increase the frequency of mIPSCs of basket and stellate cells through a presynaptic $GABA_A$ receptor due to relatively high $[Cl^-]_i$ in ML interneurons (Trigo *et al.* 2007). Because *Atp1a2*$^{-/-}$ showed significantly high $[Cl^-]_i$ in prenatal neurons due to uncoupling function between α2 subunit and neuron-specific K–Cl cotransporter 2, KCC2 (Ikeda *et al.* 2004), it is plausible that similar uncoupling occurs in the axon terminals of ML interneurons onto the Purkinje soma in *Atp1a3*$^{+/-}$, leading to enhancement of the inhibitory neurotransmission onto PCs.

How does enhanced inhibitory synaptic transmission affect cerebellar function and result in dystonia? Although we do not have a direct answer at this stage, the results of this study suggest that enhanced inhibitory synaptic transmission during the developmental stage might play a causative role. It is reported that a micromolar level of GABA that spills over from the synaptic terminals of ML interneuron–PC synapses can enhance long-term depression at neighbouring PF–PC synapses (Kamikubo *et al.* 2007). Long-term depression is one form of synaptic plasticity and crucial for cerebellar motor learning. In the case of the *Atp1a3*$^{+/-}$ cerebellum, enhanced inhibitory synaptic transmission should affect such plasticity, which might explain the persistence of symptoms of dystonia after abrupt onset. In this context, we propose that maladaptive plasticity is the main pathophysiology of dystonia (Neychev *et al.* 2011). This idea is reinforced by the reported impaired learning and memory, which are other forms of plasticity, in *Atp1a3*$^{+/-}$ (Moseley *et al.* 2007). Because *Atp1a3* is strongly expressed in PCs (Fig. 3), it is rational to speculate that properties of the inhibitory neurotransmission from PCs to deep cerebellar nucleus neurons are also changed in *Atp1a3*$^{+/-}$ (S. Satake *et al.*, unpublished data).

Atp1a3 mutant mice

Currently, three independent mouse lines harbouring mutation in *Atp1a3* are available. One is *Myshkin* (*Myk*/+), which carries an Ile→Asn (I810N) missense mutation of *Atp1a3* generated by *N*-nitroso-*N*-ethylurea (ENU) mutagenesis. Previous studies reported that I810N mutation inactivates Na pump enzymatic activity by 42% in the brain (Clapcote *et al.* 2009). *Myk*/+ mice displayed generalized seizures, and neuronal hyperexcitability (post-tetanic hyperexcitability of the CA3–CA1 hippocampal pathway), mania-like behaviour and increased susceptibility to depression-like phenotype under chronic variable stresses (Clapcote *et al.* 2009; Kirshenbaum *et al.* 2011*a*). It is noteworthy that *Myk*/+ showed degeneration of some PCs in the cerebellum. The second line is the *Atp1a3* knockout haploinsufficient mice generated by Lingrel's group (Moseley *et al.* 2007). These mice developed increased locomotion induced after injection of methamphetamine, and showed spatial learning and memory deficits. The third line is the mice described in the present study. None of these *Atp1a3* mutated mice exhibited overt dystonia. The reasons for the lack of spontaneous dystonia phenotype in *Atp1a3* mutated mice are not clear (Fremont & Khodakhah, 2012). In particular, no spontaneous motor disturbance was observed in the latter two *Atp1a3* knockout heterozygous mice lines, indicating that haploinsufficiency of the gene is not sufficient to induce evident motor symptoms, including dystonia, during the life span of mice under commonly used stress conditions and that some dominant-negative effects on the wild-type α3 subunit by mutated proteins may underlie the mechanism of onset of dystonia. Nevertheless, all three lines of *Atp1a3* mutated mice clearly exhibited changes in motor behaviour (Fig. 2; Moseley *et al.* 2007; Clapcote *et al.* 2009; Kirshenbaum *et al.* 2011*a*, 2011*b*). In addition, learning deficits in one line (Moseley *et al.* 2007) and changes in inhibitory synaptic transmission in the cerebellum (Figs 5 and 6) as well as better sense of motor balance in the present heterozygous mouse line (Fig. 2) are found. It is possible that the improved motor ability was due to increased routine practical activities during mobile-young age in the wire-roof home cage, although its relevance to clinical symptoms in humans is not clear. The other *Atp1a3*

heterozygous knockout mice developed stress-dependent motor symptoms, such as impaired motor coordination and balance, although these were noted in female mice only, but not in males (DeAndrade *et al.* 2011). The results of the rotarod test in the present study showed different behaviour in female *Atp1a3*$^{+/-}$ (Fig. 2*C*). Although we have not addressed it in males, different behaviour might be observed only in females. Related to this observation, one study reported sex-dependent effect of restraint 'stress' in mice (Koehl *et al.* 2006). To our knowledge, sex differences in *ATP1A3*$^{+/-}$ patients have not been reported. However, considering the 'stress'-induced motor deficits in RDP patients (Brashear *et al.* 2007) and certain disorders with gender variability in penetrance and expressivity (e.g. GTP cyclohydrolase 1 gene mutation known to cause fluctuating dystonia; Steinberger *et al.* 1998), behavioural studies using mice might be necessary to determine the exact differences between the two sexes and their mechanisms.

We found altered properties of inhibitory synapses of the cerebellar cortex in genetically mutated developing young heterozygous *Atp1a3* mice, even though these were prior to the manifestation of motor and behavioural changes. Our results shed light on the role of *Atp1a3* in cerebellar inhibitory neural network formation and potential involvement of inhibitory synaptic dysfunction for the pathophysiology of symptoms caused by mutations in *ATP1A3*.

References

Batchelor AM, Madge DJ & Garthwaite J (1994). Synaptic activation of metabotropic glutamate receptors in the parallel fibre–Purkinje cell pathway in rat cerebellar slices. *Neuroscience* **63**, 911–915.

Blanco-Arias P, Einholm AP, Mamsa H, Concheiro C, Gutiérrez-de-Terán H, Romero J, Toustrup-Jensen MS, Carracedo Á, Jen JC, Vilsen B & Sobrido MJ (2009). A C-terminal mutation of *ATP1A3* underscores the crucial role of sodium affinity in the pathophysiology of rapid-onset dystonia-parkinsonism. *Hum Mol Genet* **18**, 2370–2377.

Blanco G (2005). The Na/K-ATPase and its isozymes: what we have learned using the baculovirus expression system. *Front Biosci* **10**, 2397–2411.

Bøttger P, Tracz Z, Heuck A, Nissen P, Romero-Ramos M & Lykke-Hartmann K (2011). Distribution of Na/K-ATPase alpha 3 isoform, a sodium-potassium P-type pump associated with rapid-onset of dystonia parkinsonism (RDP) in the adult mouse brain. *J Comp Neurol* **519**, 376–404.

Brashear A, Dobyns WB, de Carvalho Aguiar P, Borg M, Frijns CJM, Gollamudi S, Green A, Guimaraes J, Haake BC, Klein C, Linazasoro G, Münchau A, Raymond D, Riley D, Saunders-Pullman R, Tijssen MAJ, Webb D, Zaremba J, Bressman SB & Ozelius LJ (2007). The phenotypic spectrum of rapid-onset dystonia-parkinsonism (RDP) and mutations in the *ATP1A3* gene. *Brain* **130**, 828–835.

Brashear A, Sweadner K & Ozelius L (2008). Rapid-onset dystonia-parkinsonism. In: Pagon RA, Bird TD, Dolan CR, Stephens K, Adam MP, editors. GeneReviews^{TM} [Internet]. Seattle (WA): University of Washington, Seattle; 1993-Bookshelf ID: NBK1115.

Calderon DP, Fremont R, Kraenzlin F & Khodakhah K (2011). The neural substrates of rapid-onset Dystonia-Parkinsonism. *Nat Neurosci* **14**, 357–365.

Campbell DB & Hess EJ (1998). Cerebellar circuitry is activated during convulsive episodes in the tottering (*tg/tg*) mutant mouse. *Neuroscience* **85**, 773–783.

Campbell DB & Hess EJ (1999). L-type calcium channels contribute to the tottering mouse dystonic episodes. *Mol Pharmacol* **55**, 23–31.

Chauhan N & Siegel G (1997). Differential expression of Na,K-ATPase α-isoform mRNAs in aging rat cerebellum. *J Neurosci Res* **47**, 287–299.

Clapcote SJ, Duffy S, Xie G, Kirshenbaum G, Bechard AR, Rodacker Schack V, Petersen J, Sinai L, Saab BJ, Lerch JP, Minassian BA, Ackerley CA, Sled JG, Cortez MA, Henderson JT, Vilsen B & Roder JC (2009). Mutation I810N in the α3 isoform of Na^+,K^+-ATPase causes impairments in the sodium pump and hyperexcitability in the CNS. *Proc Natl Acad Sci U S A* **106**, 14085–14090.

DeAndrade MP, Yokoi F, van Groen T, Lingrel JB & Li Y (2011). Characterization of *Atp1a3* mutant mice as a model of rapid-onset dystonia with parkinsonism. *Behav Brain Res* **216**, 659–665.

de Carvalho Aguiar P, Sweadner KJ, Penniston JT, Zaremba J, Liu L, Caton M, Linazasoro G, Borg M, Tijssen MAJ, Bressman SB, Dobyns WB, Brashear A & Ozelius LJ (2004). Mutations in the Na^+/K^+-ATPase α3 gene *ATP1A3* are associated with rapid-onset dystonia parkinsonism. *Neuron* **43**, 169–175.

Fremont R & Khodakhah K (2012). Alternative approaches to modeling hereditary dystonias. *Neurotherapeutics* **9**, 315–322.

Heinzen EL, Swoboda KJ, Hitomi Y, Gurrieri F, Nicole S, de Vries B, Tiziano FD, Fontaine B, Walley NM, Heavin S, Panagiotakaki E; European Alternating Hemiplegia of Childhood (AHC) Genetics Consortium; Biobanca e Registro Clinico per l'Emiplegia Alternante (I.B.AHC) Consortium; European Network for Research on Alternating Hemiplegia (ENRAH) for Small and Medium-sized Enterpriese (SMEs) Consortium, Fiori S, Abiusi E, Di Pietro L, Sweney MT, Newcomb TM, Viollet L, Huff C, Jorde LB, Reyna SP, Murphy KJ, Shianna KV, Gumbs CE, Little L, Silver K, Ptáček LJ, Haan J, Ferrari MD, Bye AM, Herkes GK, Whitelaw CM, Webb D, Lynch BJ, Uldall P, King MD, Scheffer IE, Neri G, Arzimanoglou A, van den Maagdenberg AM, Sisodiya SM, Mikati MA & Goldstein DB (2012). De novo mutations in *ATP1A3* cause alternating hemiplegia of childhood. *Nat Genet* **44**, 1030–1034.

Hieber V, Siegel GJ, Desmond T, Lee-Hwa Liu J & Ernst SA (1989). Na,K-ATPase: comparison of the cellular localization of α-subunit mRNA and polypeptide in mouse cerebellum, retina, and kidney. *J Neurosci Res* **23**, 9–20.

Hieber V, Siegel GJ, Fink DJ, Beaty MW & Mata M (1991). Differential distribution of (Na, K)-ATPase α isoforms in the central nervous system. *Cell Mol Neurobiol* **11**, 253–262.

Hirono M, Konishi S & Yoshioka T (1998). Phospholipase C-independent group I metabotropic glutamate receptor-mediated inward current in mouse Purkinje cells. *Biochem Biophys Res Commun* **251**, 753–758.

Hirono M & Obata K (2006). α-Adrenoceptive dual modulation of inhibitory GABAergic inputs to Purkinje cells in the mouse cerebellum. *J Neurophysiol* **95**, 700–708.

Ichise T, Kano M, Hashimoto K, Yanagihara D, Nakao K, Shigemoto R, Katsuki M & Aiba A (2000). mGluR1 in cerebellar Purkinje cells essential for long-term depression, synapse elimination, and motor coordination. *Science* **288**, 1832–1835.

Ikeda K, Onaka T, Yamakado M, Nakai J, Ishikawa T, Taketo MM & Kawakami K (2003). Degeneration of the amygdala/piriform cortex and enhanced fear/anxiety behaviors in sodium pump α2 subunit (*Atp1a2*)-deficient mice. *J Neurosci* **23**, 4667–4676.

Ikeda K, Onimaru H, Yamada J, Inoue K, Ueno S, Onaka T, Toyoda H, Arata A, Ishikawa T, Taketo MM, Fukuda A & Kawakami K (2004). Malfunction of respiratory-related neuronal activity in Na^+,K^+-ATPase α2 subunit-deficient mice is attributable to abnormal Cl^- homeostasis in brainstem neurons. *J Neurosci* **24**, 10693–10701.

Ikeda K, Ookawara S, Sato S, Ando Z, Kageyema R & Kawakami K (2007). *Six1* is essential for early neurogenesis in the development of olfactory epithelium. *Dev Biol* **311**, 53–68.

Jewell EA & Lingrel JB (1991). Comparison of the substrate dependence properties of the rat Na,K-ATPase α1, α2, and α3 isoforms expressed in HeLa cells. *J Biol Chem* **266**, 16925–16930.

Jörntell H, Bengtsson F, Schonewille M & De Zeeuw CI (2010). Cerebellar molecular layer interneurons – computational properties and roles in learning. *Trends Neurosci* **33**, 524–532.

Kamikubo Y, Tabata T, Kakizawa S, Kawakami D, Watanabe M, Ogura A, Iino M & Kano M (2007). Postsynaptic $GABA_B$ receptor signalling enhances LTD in mouse cerebellar Purkinje cells. *J Physiol* **585**, 549–563.

Kim SJ, Kim YS, Yuan JP, Petralia RS, Worley PF & Linden DJ (2003). Activation of the TRPC1 cation channel by metabotropic glutamate receptor mGluR1. *Nature* **426**, 285–291.

Kirshenbaum GS, Saltzman K, Rose B, Petersen J, Vilsen B & Roder JC (2011*a*). Decreased neuronal Na^+,K^+-ATPase activity in *Atp1a3* heterozygous mice increases susceptibility to depression-like endophenotypes by chronic variable stress. *Genes Brain Behav* **10**, 542–550.

Kirshenbaum GS, Clapcote SJ, Duffy S, Burgess CR, Petersen J, Jarowek KJ, Yücel YH, Cortez MA, Snead III OC, Vilsen B, Peever JH, Ralph MR & Roder JC (2011*b*). Mania-like behavior induced by genetic dysfunction of the neuron-specific Na^+,K^+-ATPase α3 sodium pump. *Proc Natl Acad Sci U S A* **108**, 18144–18149.

Kodama T, Itsukaichi-Nishida Y, Fukazawa Y, Wakamori M, Miyata M, Molnar E, Mori Y, Shigemoto R & Imoto K (2006). A $Ca_v2.1$ calcium channel mutation *rocker* reduces the number of postsynaptic AMPA receptors in parallel fiber-Purkinje cell synapses. *Eur J Neurosci* **24**, 2993–3007.

Koehl M, Battle S & Meerlo P (2006). Sex differences in sleep: the response to sleep deprivation and restraint stress in mice. *Sleep* **29**, 1224–1231.

Lingrel JB & Kuntzweiler T (1994). Na^+,K^+-ATPase. *J Biol Chem* **269**, 19659–19662.

Mitoma H & Konishi S (1999). Monoaminergic long-term facilitation of GABA-mediated inhibitory transmission at cerebellar synapses. *Neuroscience* **88**, 871–883.

Matsushita K, Wakamori M, Rhyu IJ, Arii T, Oda S, Mori Y & Imoto K (2002). Bidirectional alterations in cerebellar synaptic transmission of *tottering* and *rolling* Ca^{2+} channel mutant mice. *J Neurosci* **22**, 4388–4398.

Moseley AE, Lieske SP, Wetzel RK, James PF, He S, Shelly DA, Paul RJ, Boivin GP, Witte DP, Ramirez JM, Sweadner KJ & Lingrel JB (2003). The Na,K-ATPase α2 isoform is expressed in neurons, and its absence disrupts neuronal activity in newborn mice. *J Biol Chem* **278**, 5317–5324.

Moseley AE, Williams MT, Schaefer TL, Bohanan CS, Neumann JC, Behbehani MM, Vorhees CV & Lingrel JB (2007). Deficiency in Na,K-ATPase α isoform genes alters spatial learning, motor activity, and anxiety in mice. *J Neurosci* **27**, 616–626.

Neychev VK, Fan X, Mitev VI, Hess EJ & Jinnah HA (2008). The basal ganglia and cerebellum interact in the expression of dystonic movement. *Brain* **131**, 2499–2509.

Neychev VK, Gross RE, Lehéricy S, Hess EJ & Jinnah HA (2011). The functional neuroanatomy of dystonia. *Neurobiol Dis* **42**, 185–201.

Niethammer M, Carbon M, Argyelan M & Eidelberg D (2011). Hereditary dystonia as a neurodevelopmental circuit disorder: evidence from neuroimaging. *Neurobiol Dis* **42**, 202–209.

Ozelius LJ (2012). Clinical spectrum of disease associated with *ATP1A3* mutations. *Lancet Neurol* **11**, 741–743.

Partin KM, Patneau DK, Winters CA, Mayer ML & Buonanno A (1993). Selective modulation of desensitization at AMPA versus kainate receptors by cyclothiazide and concanavalin A. *Neuron* **11**, 1069–1082.

Phukan J, Albanese A, Gasser T & Warner T (2011). Primary dystonia and dystonia-plus syndromes: clinical characteristics, diagnosis, and pathogenesis. *Lancet Neurol* **10**, 1074–1085.

Pizoli CE, Jinnah HA, Billingsley ML & Hess EJ (2002). Abnormal cerebellar signaling induces dystonia in mice. *J Neurosci* **22**, 7825–7833.

Pressley TA (1992). Phylogenetic conservation of isoform-specific regions within α-subunit of Na^+-K^+-ATPase. *Am J Physiol* **262**, C743–C751.

Pouzat C & Hestrin S (1997). Developmental regulation of basket/stellate cell→Purkinje cell synapses in the cerebellum. *J Neurosci* **17**, 9104–9112.

Rodacker V, Toustrup-Jensen M & Vilsen B (2006). Mutations Phe785Leu and Thr618Met in Na^+,K^+-ATPase, associated with familial rapid-onset dystonia parkinsonism, interfere with Na^+ interaction by distinct mechanisms. *J Biol Chem* **281**, 18539–18548.

Rosewich H, Thiele H, Ohlenbusch A, Maschke U, Altmüller J, Frommolt P, Zirn B, Ebinger F, Siemes H, Nürnberg P, Brockmann K & Gärtner J (2012). Heterozygous de-novo mutations in *ATP1A3* in patients with alternating hemiplegia of childhood: a whole-exome sequencing gene-identification study. *Lancet Neurol* **11**, 764–773.

Saitow F, Satake S, Yamada J & Konishi S (2000). β-Adrenergic receptor-mediated presynaptic facilitation of inhibitory GABAergic transmission at cerebellar interneuron-Purkinje cell synapses. *J Neurophysiol* **84**, 2016–2025.

Satake S, Saitow F, Yamada J & Konishi S (2000). Synaptic activation of AMPA receptors inhibits GABA release from cerebellar interneurons. *Nat Neurosci* **3**, 551–558.

Satake S, Song S-Y, Konishi S & Imoto K (2010). Glutamate transporter EAAT4 in Purkinje cells controls intersynaptic diffusion of climbing fiber transmitter mediating inhibition of GABA release from interneurons. *Eur J Neurosci* **32**, 1843–1853.

Segall L, Daly SE & Blostein R (2001). Mechanistic basis for kinetic differences between the rat α1, α2, and α3 isoforms of the Na,K-ATPase. *J Biol Chem* **276**, 31535–31541.

Sotelo C (2008). Development of 'pinceaux' formations and dendritic translocation of climbing fibers during the acquisition of the balance between glutamatergic and γ-aminobutyric acidergic inputs in developing Purkinje cells. *J Comp Neurol* **506**, 240–262.

Steinberger D, Weber Y, Korinthenberg R, Deuschl G, Benecke R, Martinius J & Müller U (1998). High penetrance and pronounced variation in expressivity of *GCH1* mutations in five families with Dopa-responsive dystonia. *Ann Neurol* **43**, 634–639.

Takayama C & Inoue Y (2004). Extrasynaptic localization of GABA in the developing mouse cerebellum. *Neurosci Res* **50**, 447–458.

Trigo FF, Chat M & Marty A (2007). Enhancement of GABA release through endogenous activation of axonal $GABA_A$ receptors in juvenile cerebellum. *J Neurosci* **27**, 12452–12463.

Wadiche JI & Jahr CE (2001). Multivesicular release at climbing fiber-Purkinje cell synapses. *Neuron* **32**, 301–313.

Wadiche JI & Jahr CE (2005). Patterned expression of Purkinje cell glutamate transporters controls synaptic plasticity. *Nat Neurosci* **8**, 1329–1334.

Watanabe M & Kano M (2011). Climbing fiber synapse elimination in cerebellar Purkinje cells. *Eur J Neurosci* **34**, 1697–1710.

Yagi T, Tokunaga T, Furuta Y, Nada S, Yoshida M, Tsukada T, Saga Y, Takeda N, Ikawa Y & Aizawa S (1993). A novel ES cell line, TT2, with high germline-differentiating potency. *Anal Biochem* **214**, 70–76.

Zucker RS & Regehr WG (2002). Short-term synaptic plasticity. *Annu Rev Physiol* **64**, 355–405.

Additional information

Competing interests

None.

Author contributions

The experiments were performed at the laboratory of K.K., T.O. and K. Imoto. Conception and design of experiments and drafting the article: K.K. and K.I. Collection, analysis and interpretation of data and drafting the article: S.S., T.O., H.S. and K.I. Development of knockout mice: N.T. Supervision of experiments and critical revision of the article: K. Imoto.

Funding

This work was supported by the Brain Science Foundation (K.I.), The Kato Memorial Trust for Nambyo Research (K.I.), and by JSPS KKENHI Grant Number 21590239 (K.K.) and MEXT-Supported Program for the Strategic Research Foundation at Private Universities, 2008–2012.

Acknowledgements

We thank all members of the Division of Biology for the helpful discussion and technical assistance. The authors declare no conflict of interest.